BIOCHEMISTRY
including biophysical chemistry & molecular biology

Article

pubs.acs.org/biochemistry

In Vitro Selection and Characterization of a Novel Zn(II)-Dependent Phosphorothiolate Thiolesterase Ribozyme

Tzu-Pin Wang,*[,†] Yu-Chih Su,[†] Yi Chen,[†] Yi-Ming Liou,[†] Kun-Liang Lin,[†] Eng-Chi Wang,[†] Long-Chih Hwang,[†] Yun-Ming Wang,[§] and Yen-Hsu Chen[‡,∥]

[†]Department of Medicinal and Applied Chemistry and [‡]Graduate Institute of Medicine, Kaohsiung Medical University, Kaohsiung 80708, Taiwan

[§]Department of Biological Science and Technology, National Chiao Tung University, Hsin-Chu 300, Taiwan

[∥]Department of Internal Medicine, Kaohsiung Medical University Hospital, Kaohsiung 80708, Taiwan

Supporting Information

ABSTRACT: Here we present the in vitro selection of a novel ribozyme specific for Zn^{2+}-dependent catalysis on hydrolysis of a phosphorothiolate thiolester bond. The ribozyme, called the TW17 ribozyme, was evolved and selected from an artificial RNA pool covalently linked to a biotin-containing substrate through the phosphorothiolate thiolester bond. The secondary structure for the evolved ribozyme consisted of three major helices and three loops. Biochemical and chemical studies of ribozyme-catalyzed reaction products provided evidence that the ribozyme specifically catalyzes hydrolysis of the phosphorothiolate thiolester linkage. A successful ribozyme construct with active catalysis in trans further supported the determined ribozyme structure and indicated the potential of the ribozyme for multiple-substrate turnover. The ribozyme also requires Zn^{2+} and Mg^{2+} for maximal catalysis. The TW17 ribozyme, in the presence of Zn^{2+} and Mg^{2+}, conferred a rate enhancement of at least 5 orders of magnitude when compared to the estimated rate of the uncatalyzed reaction. The ribozyme completely lost catalytic activity in the absence of Zn^{2+}, like Zn^{2+}-dependent protein hydrolases. The discovery and characterization of the TW17 ribozyme suggest additional roles for Zn^{2+} in ribozyme catalysts.

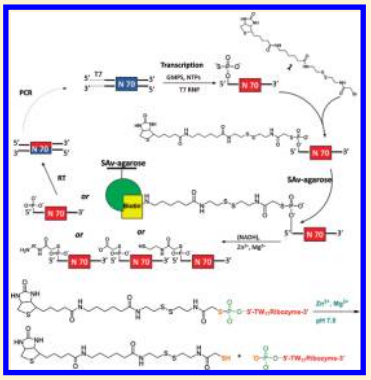

The discovery of RNA catalysts (ribozymes) for accelerating chemical reactions in modern biological systems[1,2] has led to the postulation of "the RNA world" hypothesis in which RNA molecules undertook dual critical functions in primordial life: biological catalysts and genetic information carriers.[3] Convincing evidence to support the RNA world hypothesis has been provided by the development of Darwinian-like in vitro evolution and selection approaches to obtaining ribozymes from artificial RNA pools in laboratories.[4−6] These in vitro-selected ribozymes have been shown to catalyze diverse chemical reactions, including alkylation,[7,8] the Diels−Alder cycloaddition,[9] the Michael addition,[10] the aldol condensation,[11] NAD^+-dependent alcohol dehydrogenation,[12] and NADH-dependent aldehyde hydrogenation.[13] Currently, the number and type of chemical transformations catalyzed by ribozymes do not match the number and type of modern protein enzymes. However, the intricate metabolic reactions present in the contemporary protein-dominated world could be derived from analogous reactions in the primitive RNA world as modern complex life is suggested to gradually evolve from the RNA world.[14,15] Moreover, RNA and protein enzymes might exploit similar catalytic chemistry to increase the rates for the same chemical reactions even though they have fundamental structural differences. For example, in modern biological systems, zinc is the only metal present in all six classes of the International Union of Biochemistry (IUB) enzymes.[16,17] The preference of protein enzymes for Zn^{2+} as a cofactor to catalyze diverse chemical reactions alludes to possible similar catalytic roles of zinc in the RNA world.

The presence of natural and nonnatural Zn^{2+}-assisted or Zn^{2+}-dependent nucleic acid enzymes sheds light on plausible catalytic functions of zinc in primordial life metabolism. Ribozymes in the presence of Zn^{2+} catalyze chemical reactions encompassing transesterification of RNA phosphodiester linkages by hammerhead ribozymes,[18,19] dehydrogenation of alcohol by an alcohol dehydrogenase ribozyme,[12] reduction of aldehyde by the same alcohol dehydrogenase ribozyme,[13] phosphodiester hydrolysis by *Escherichia coli* RNase P RNA,[20,21] and an aldol reaction by an aldolase ribozyme.[11] A Zn^{2+}-dependent deoxyribozyme also catalyzes transesterification reactions to cleave RNA or DNA−RNA chimeric substrates.[22] All reactions that include Zn^{2+} catalyzed by nucleic acids can find their counterparts in the Zn^{2+}-dependent protein enzymes of modern living organisms. Identification of Zn^{2+}-dependent ribozymes may be crucial in reconstructing the proposed RNA world and provide insight into the evolution of life ascending from an RNA world.

Received: October 15, 2011
Revised: December 6, 2011
Published: December 16, 2011

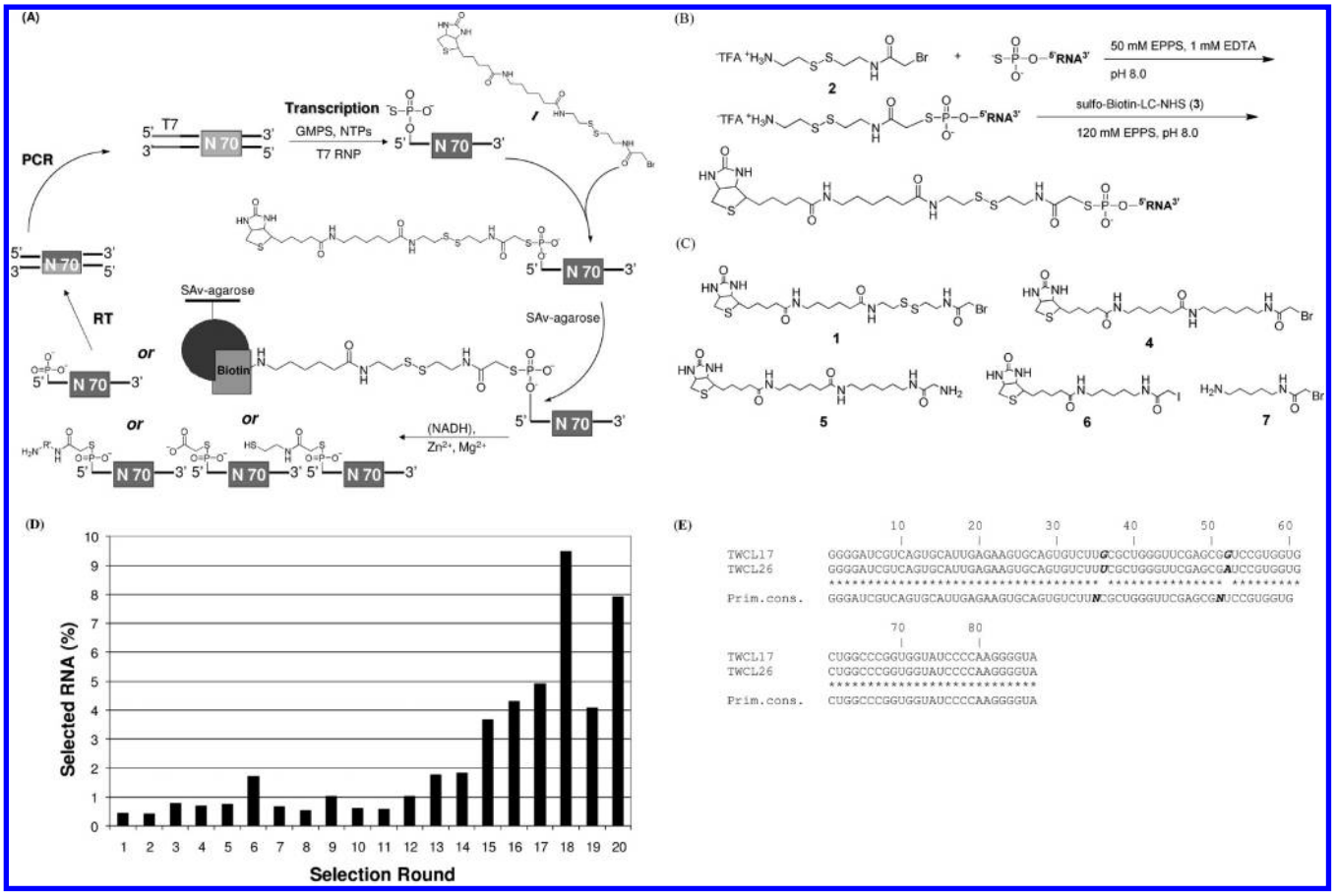

Figure 1. (A) Strategies for the selection of Zn^{2+}-dependent hydrolase and NADH-dependent disulfide reductase ribozymes. Gray and black boxes indicate the random region of DNA and RNA sequences, respectively. For the sake of simplicity, full-length substrate **1** is shown to be linked to GMPS-primed RNA pools by one conjugation reaction. RNA pools were actually conjugated with **2** first, followed by conjugation of the product with **3** to give desired RNA−substrate **1** conjugate pools (see panel B). Abbreviations: RT, reverse transcription; PCR, polymerase chain reaction; N70, random sequence region 70 nucleotides in length; T7 RNP, T7 RNA polymerase; NTPs, nucleoside triphosphates; SAv-agarose, streptavidin−agarose beads. (B) Preparation of RNA−substrate **1** conjugate pools for in vitro selection. (C) Structures of several substrates for screening catalytic activity in RNA and probing substrate specificity in TW17 ribozyme catalysis. (D) Active RNA sequence enrichment during in vitro evolution and selection. The stringency of the selection was increased stepwise, including round 7 for reducing the reaction time from 24 to 3 h and round 10 for reducing the reaction time from 3 to 0.5 h. Note that 1 mM NADH was used in the selection reactions in rounds 1−13 but no NADH was added after the selection of round 13. (E) Sequence alignment for the TW17 and TW26 RNA in which the locations of nucleotides with sequence heterogeneity are italicized and bolded.

Here we report the in vitro selection of a novel ribozyme that is able to catalyze hydrolysis of a phosphorothiolate thiolester bond in the presence of Zn^{2+}. The phosphorothiolate thiolesterase RNA, called the TW17 ribozyme, evolved from an artificial RNA pool covalently linked with a biotin derivative substrate **1** through a phosphorothiolate thiolester bond (Figure 1A−C and Figure S1A,B of the Supporting Information). Site-directed mutagenesis studies of the 87-nucleotide (nt) TW17 ribozyme provided the structure−activity relationships and led to the determination of the three-helix secondary structure for the ribozyme. Comprehensive biochemical and chemical analyses of ribozyme-catalyzed reaction products provide conclusive evidence that the TW17 ribozyme specifically catalyzes hydrolysis of the phosphorothiolate thiolester linkage. Moreover, a successful TW17 ribozyme construct with active catalysis in trans further supports the determined ribozyme structure and unveils the potential of the ribozyme for multiple-substrate turnover. TW17 ribozyme catalysis also demonstrates the indispensable roles of Zn^{2+} cofactors and requires the simultaneous presence of Zn^{2+} and Mg^{2+} to attain maximal catalysis. The discovery of the TW17 ribozyme provides further evidence of the diverse role of Zn^{2+} in ribozyme catalysis and may have implications for RNA-based metabolic systems in primordial life.

MATERIALS AND METHODS

Materials. DNA oligonucleotides were purchased from Purigo Biotech, Inc. (Taiwan), and purified by denaturing urea (8 M)−polyacrylamide gel electrophoresis (PAGE). All reagents were purchased from commercial sources (Sigma-Aldrich, Acros, Alfa Aesar, Mallinckrodt Baker, and Merck KGaA) except where noted and were further purified as necessary. RNA samples were analyzed by urea−PAGE or a streptavidin (SAv) gel shift assay in urea−PAGE, visualized, and quantified with an Amersham Typhoon PhosphorImager system (GE Healthcare Bio-Sciences AB, Uppsala, Sweden). Synthesis of substrates for selection and characterization of the ribozyme will be described elsewhere.

Oligonucleotide Preparation of *cis*-Acting TW17 RNA Molecules. The TW17 DNA (5′-GGTAACACGCATATG-TAATACGACTCACTATAGGGATCGTCAGTGCATTGA-

GAATGTCAGTGTCTTGCGCTGGGTTC-GAGCGGTCCGTGGTGCTGGCCCGGTGGTATCCC-CAAGGGGTA-3′) was amplified from a plasmid containing the cloned DNA using the normal 5′ end primer (5′-AACACGCATATGTAATACGACTCACTATAGG-GATCGTCAGTGCATTGAG-3′) and the normal 3′ end primer (5′-TACCCCTTGGGGATACCACC-3′). Polymerase chain reactions (PCRs) for DNA extension or amplification were performed using standard protocols to prepare the TW17 DNA and its mutants. A list of DNA primers for the preparation of seven representative TW17 DNA mutants is also provided in the Supporting Information (Table S1). PCR products were purified by phenol/chloroform extraction, ethanol precipitation, and redissolution in 50 mM KCl.

RNA was transcribed from PCR-amplified double-stranded DNA carrying the T7 promoter sequence using the T7 RNA polymerase runoff reaction with ATP, CTP, GTP, and UTP (6.25 mM each), 4 mM GMPS (guanosine α-thiomonophosphate), and 5 μCi of [α-^{32}P]GTP/UTP (Izotop, Hungary). After the treatment of RQ1 DNase (Promega, Madison, WI) at 37 °C for 10 min, the GMPS-primed RNA transcript was purified by one denaturing PAGE and one denaturing [(*N*-acryloylamino)phenyl]mercury (APM) PAGE,[23] eluted from the ground gel by being rotated in the presence of 0.3 M NaCl with or without 0.1 M DTT for 1 h at 25 °C, and precipitated with ethanol twice after each denaturing PAGE purification. The acquired GMPS-primed RNA was quantified by the measurement of A_{260}. Guanosine monophosphate (GMP)-primed RNA was synthesized by modifying the method for GMPS-primed RNA with 4 mM GMPS substituted with 10 mM GMP during the T7 RNA polymerase runoff transcription. ^{32}P-body-labeled GMP-primed RNA was purified by 8% denaturing urea−PAGE, eluted from the ground gel by being rotated in the presence of 0.3 M NaCl for 1 h at 25 °C, precipitated with ethanol, washed with 70% ethanol, and resuspended in DEPC water. The acquired GMP-primed RNA was also quantified by the measurement of A_{260}. GTP-primed RNA was synthesized using a similar T7 RNA polymerase runoff reaction without either GMPS or GMP.

In Vitro Selection. The initial DNA pool for RNA selection consisted of a 70-nt random sequence flanked by 20-nt constant sequences at the 5′ and 3′ ends (5′-GGATCGT-CAGTGCATTGAGA-N70-GGTGGTATCCCCAAGGGG-TA-3′) and was prepared as previously described (Figure 1A).[12] The DNA pool (complexity of 1.6×10^{15}; four copies of each DNA) was transcribed and purified by 10% denaturing urea−PAGE to afford a GMPS-primed RNA pool doped with RNA body labeled with [α-^{32}P]GTP for the first round of selection. RNA pools body-labeled with [α-^{32}P]GTP were prepared and used from the onset of the second round of selection. Conjugation of the GMPS-primed RNA pool with the pro-substrate **2** was conducted via a reaction mixture containing 5 μM GMPS-primed RNA, 5 mM substrate **2**, and 10% (v/v) DMF in EE buffer [50 mM *N*-(2-hydroxyethyl)piperazine-*N*′-3-propanesulfonic acid (EPPS) and 1 mM EDTA (pH 8.0)] (Figure 1B). The reaction proceeded at 25 °C for 3 h, after which the reaction products were precipitated with ethanol twice to isolate a **2**−RNA pool. The **2**−RNA pool was further biotinylated with 9 mM sulfo-NHS-LC-biotin (**3**) (Pierce, Rockford, IL) at 25 °C for 1 h to afford the **1**−RNA pool according to a modified method of Pütz et al.[24] (Figure 1B). The biotinylation had an efficiency of 70% as shown by a SAv gel shift assay via 8% urea−PAGE (T.-P. Wang et al., unpublished results). The acquired **1**−RNA pool was the starting material in each selection round.

Each selection began by application of a biotinylated **1**−RNA pool to a column containing 50 μL (400 μL for the first round) of SAv-agarose resin (Pierce) in which the column was previously blocked with 200 μL of 0.2 μM blocking RNA (in EE buffer) for 1 h. The RNA slurry was gently rocked for 30 min at 25 °C to ensure maximal biotinylated RNA binding and was extensively washed twice with 20 resin volumes of 4 M urea and twice with 5 resin volumes of EPPS buffer [50 mM EPPS (pH 8.0)] sequentially to remove nonbiotinylated RNA from the column. The resulting slurry was transferred to a microfuge tube containing 60 μL of EK buffer [50 mM EPPS and 500 mM KCl (pH 7.5); 150 μL for the first round] and 48 μL of DEPC water (120 μL for the first round). The RNA-containing slurry was denatured at 95 °C for 2−3 min and annealed at 25 °C for 10−15 min, and Mg^{2+} (100 mM) and Zn^{2+} (0.5 mM) were added sequentially. The slurry was immediately transferred back to the column and washed with 2 resin volumes of EKMZ buffer [100 mM EPPS, 1 M KCl, 100 mM Mg^{2+}, and 0.5 mM Zn^{2+} (pH 7.5)] to elute any unbound RNA.

In rounds 1−13, the selection reaction was achieved via the addition of 2 resin volumes of 1 mM NADH in EKMZ buffer with stepwise reduction of the incubation time in the dark (rounds 1−6, 24 h; rounds 7−9, 3 h; rounds 10−13, 30 min); the slurry was washed twice with 2 resin volumes of EKMZ buffer, and the eluates were collected. NADH was incorporated into the reaction mixture as a reductant to facilitate isolation of disulfide reductase RNA. The eluted RNA was converted to cDNA by reverse transcription [M-MLV reverse transcriptase (Promega)], according to the manufacturer's protocol. The acquired cDNA was then amplified by PCR to prepare the DNA pool for the next round of selection.

In round 14, the selection reaction was performed in two stages with the first-stage reaction being incubation of the slurry with 2 resin volumes of EKMZ buffer for 30 min in the dark. In the second-stage reaction, the same slurry was incubated with 2 resin volumes of 1 mM NADH in EKMZ buffer for 30 min in the dark. The slurry was extensively washed five times with 2 resin volumes of EKMZ buffer after each stage reaction; the eluted RNA from each stage reaction was separately collected and pooled. Two RNA pools were obtained from the round 14 selection: a NADH-independent pool from the EKMZ buffer incubation reaction and a NADH-dependent pool from the 1 mM NADH in EKMZ buffer incubation reaction.

The NADH-independent pool was subjected to six more rounds of selection. The selection reaction in each round was performed by incubation of the slurry with 2 resin volumes of EKMZ buffer for 30 min in the dark; the slurry was washed twice with 2 resin volumes of EKMZ buffer, and the eluates were collected.

The eluted RNA from round 20 was reversely transcribed, amplified, elongated at the 3′ end by PCR, and cloned to the pGEM-T vector (Promega) according to the manufacturer's protocol. Fifty clones were randomly picked from master plates, and the inserted DNA in each clone was amplified by PCR, transcribed to the corresponding RNA, and screened for the phosphorothiolate thiolesterase activity in each RNA. The phosphorothiolate thiolesterase activity of RNA was determined by measuring the change in cleavage percentage of the refolded RNA−**1** conjugate in EKMZ buffer after reaction for 2 h.

Direct Conjugation of the GMPS-Primed TW17 RNA with Substrates 1, 4, 6, and 7. Direct conjugation of the GMPS-primed TW17 RNA with **1** was conducted in EE buffer containing 1.2 μM GMPS-primed RNA, 30 mM substrate **1** (in DMF), 30% DMF, and 4 mM tris(2-carboxyethyl)phosphine (TCEP) (Figure S1A of the Supporting Information). The reaction mixture was incubated at 25 °C for 3 h, and the resulting TW17 RNA−**1** conjugate was purified twice by ethanol precipitation. The same procedures were used to conjugate the GMPS-primed TW17 RNA with **6** [iodoacetyl-LC-biotin (Pierce)] by substituting for **1**. Substrate **4** was also conjugated to the GMPS-primed TW17 RNA by a similar method in which 7.2 mM **4** (in DMF) and 36% DMF were used in the reaction. Direct conjugation of the GMPS-primed TW17 RNA with **7** was achieved with a reaction mixture containing 2.84 μM GMPS-primed RNA, 5 mM **7** (in DMF), 10% DMF, 2 mM TCEP, and EE buffer. The reaction was stopped after 3 h at 25 °C, and the resulting TW17 RNA−**7** conjugate was purified twice by ethanol precipitation. Direct conjugation of the GMPS-primed TW17 RNA with bromoacetate was performed by preparing a reaction solution containing 0.5 μM GMPS-primed RNA, 20 mM bromoacetic acid (in DMF), 20% DMF, 2 mM TCEP, and PE buffer [100 mM PIPES (1,4-piperazinediethanesulfonic acid) and 2 mM EDTA (pH 7.0)]. The reaction was stopped after 3 h at 25 °C and the mixture purified twice by ethanol precipitation to afford the TW17 RNA−acetate conjugate. The efficiency of formation of the TW17 RNA−**1** conjugate was analyzed by 10% APM−urea−PAGE, which indicated quantitative yields for the conjugate (Figure S1B of the Supporting Information). Similar quantitative yields were also obtained when the GMPS-primed TW17 RNA formed conjugates with other substrates (T.-P. Wang et al., unpublished results).

Procedures of the Phosphoramidation Reaction To Conjugate the GMP-Primed TW17 RNA with Substrate 5. The phosphoramidation reaction was based on a previously reported method[25] and conducted by dissolving GMP-primed RNA (92 pmol) and EDC (6.52 μmol) in 20 μL of UI buffer [8 M urea and 0.1 M imidazole (pH 6.0)] and activating at 25 °C for 10 min. Addition of 7.5 μL of UEE buffer [8 M urea, 50 mM EPPS, and 1 mM EDTA (pH 8.0)] and 5 μL of **5** (28.8 mM in DMF) followed, and the mixture was allowed to react at 41 °C for 3 h. The resulting RNA−substrate conjugate was purified twice by ethanol precipitation, separated by a SAv gel shift assay via 8% urea−PAGE, and analyzed with an Amersham Typhoon PhosphorImager system, affording an 80% yield.

Purification of *cis*-Acting TW17 Ribozyme Catalysis Products. Products from the reaction catalyzed by the *cis*-acting TW17 ribozymes were dissolved in 50 μL of binding buffer [25 mM EPPS and 1 mM EDTA (pH 7.5)] and loaded onto a column containing 50 μL of thiopropyl-activated resin (Sigma) previously blocked with 200 μL of 0.2 μM blocking RNA (in EE buffer) for 1 h. The RNA slurry was rocked using gentle agitation for 1 h at room temperature. The resulting resin was eluted and extensively washed with 2−5 volumes of washing buffer [25 mM EPPS, 1 M NaCl, and 5 mM EDTA (pH 7.5)]. The eluted RNA was pooled, purified by ethanol precipitation, redissolved in 50 μL of EKE buffer [50 mM EPPS, 500 mM KCl, and 5 mM EDTA (pH 7.5)], and loaded into a column containing 50 μL of SAv-agarose resin (Pierce) that also had been previously blocked with 200 μL of 0.2 μM blocking RNA (in EE buffer) for 1 h. The RNA slurry was again gently rocked for 30 min at 25 °C to ensure maximal biotinylated RNA binding and was washed twice with 2 resin volumes of EKE buffer. The eluted RNA from the EKE buffer wash was collected, pooled, and purified by ethanol precipitation as previously described to afford the purified TW17 ribozyme reaction product.

Product Analysis. The products from the ^{32}P-labeled TW17 ribozyme-catalyzed reaction were analyzed by high-resolution urea−PAGE and two-dimensional thin layer chromatography (2D TLC). Prior to the analysis, compounds including bromoacetate, **4** and **7**, were covalently linked to the GMPS-primed TW17 ribozyme to afford the corresponding conjugates. High-resolution urea−PAGE was performed in 8−10% urea−PAGE sequencing gels run at 90 W for 5−6 h. For 2D TLC, the reaction mixture of *cis*-acting TW17 ribozyme catalysis was digested with 2.5 units of RNase T2 (Sigma) in 50 mM sodium acetate (pH 5.3) at 50 °C for 2.5 h and then spotted onto a cellulose TLC plate [10 cm × 10 cm, Silica gel 60 F_{254} (Merck KGaA, Darmstadt, Germany)]. RNase T2 digestion was also performed on the GMPS-primed TW17 ribozyme, the GMP-primed TW17 ribozyme, the GMPS-primed TW17 ribozyme conjugated with bromoacetate, and the column-purified reaction products from the *cis*-acting TW17 ribozyme catalysis described above. All TLC plates were wet in a solution containing a 10:1 H_2O/saturated $(NH_4)_2SO_4$ mixture and dried in vacuo for 12 h before application of a roughly 2000 cpm ^{32}P-labeled RNA sample to each plate. The first axis for the 2D TLC analysis was run in 70% ethanol; after the sample had been dried in vacuo for 12 h, the second axis was run in a 40:1 saturated $(NH_4)_2SO_4$/2-propanol mixture.[26] After the 2D TLC analysis, the RNA samples were visualized with an Amersham Typhoon PhosphorImager system.

Biotin-containing reaction products from the reaction catalyzed by the *cis*-acting and *trans*-acting TW17 ribozymes were analyzed by ESI-MS. Prior to ESI-MS analyses, each sample was prepared first by removal of the RNA from the reaction mixtures through ethanol precipitation in the presence of 0.3 M NaCl. The supernatant was transferred to a clean microfuge tube, dried, and redissoved in 360 μL of dichloromethane. The supernatant was again transferred to a clean microfuge tube, dried, and redissolved in a suitable amount of HPLC-grade methanol before ESI-MS analyses. Samples were analyzed with a Waters LC-MS system (Waters, Milford, MA; Kaohsiung Medical University) equipped with a Waters Micromass ZQ detector and a Waters 2695 Separations Module using flow injection analysis. The cone voltage was set at 25 V.

General Kinetic Assays. The TW17 ribozyme catalysis was performed in a reaction mixture containing 1 μM ^{32}P-body-labeled ribozyme, 100 mM $MgCl_2$, and 0.5 mM $ZnCl_2$ in EK buffer. Before catalysis, the TW17 ribozyme was heated at 95 °C for 1 min, spun down, and cooled at room temperature for 10 min in the absence of the metal ions. Mg^{2+} and Zn^{2+} were then added sequentially to the RNA solution at the indicated concentrations to initiate TW17 ribozyme catalysis. Aliquots were removed from the reaction mixture at specific times during the course of the reaction. After the samples had been purified with two ethanol precipitations, the samples were separated by a SAv gel shift assay via 8% urea−PAGE and analyzed with an Amersham Typhoon PhosphorImager system. The obtained data were fitted to a single-exponential equation for first-order kinetics [$F(t) = F_0 + F_{max}(1 - e^{-k_{obs}t})$, where $F(t)$ is the percent cleavage of the reactant at time t] to afford the first-order rate constant, k_{obs} (GraphPad, La Jolla, CA).

Preparation of RNA Molecules for the *trans*-Phosphorothiolate Thiolesterase Assay. The TW17 ribozyme was dissected into two parts: a substrate-bearing S_{1-18} RNA containing the first 18 nucleotides in the TW17 ribozyme and a mini catalytic $TW17_{22-87}$ ribozyme with a truncation of the first 21 nucleotides of the TW17 ribozyme. The S_{1-18} DNA was amplified from a DNA template (TC-20, 5′-AAC ACG CAT ATG TAA TAC GAC TCA CTA TA G GGA TCG TCA GTG CAT TG-3′) by the standard PCR protocol using the shortened normal 5′ primer (Table S1 of the Supporting Information) and an 18-mer 3′ primer (TC-21, 5′-CAAT GCA CTG ACG ATC CC-3′). The $TW17_{22-87}$ DNA was generated from two reactions briefly described below. The first reaction was an extension reaction in which two primers (TC-2, 5′-AACACG-C A T A T G T A A T A C G A C T C A C T A T A A G T G -CAGT**GTCTTGCGCTG**-3′; TC-3, 5′-CACCGGGCCAG-CACCACGGACCGCTCGAACC**CAGCGCAAGAC**-3′) hybridized each other in the bolded and underlined sequences and were subjected to one round of an extension PCR with no addition of other primers. DNA from the extension reaction served as the DNA template for the second reaction, a standard PCR using the primer pair of the TC-2 primer and the normal 3′-35 primer (Table S1 of the Supporting Information). The PCR products were purified by phenol/chloroform extraction and ethanol precipitation and redissolved in 50 mM KCl. The ^{32}P-body-labeled GMPS-primed S_{1-18} RNA was synthesized using the previously described T7 RNA polymerase runoff reaction with 8 mM GMPS, an optimal concentration and 2 times the GMPS concentration used in the standard transcription reaction described above. The GMPS-primed S_{1-18} RNA was also conjugated with **4** by the method previously described. The cold $TW17_{22-87}$ ribozyme was also synthesized by the same T7 RNA polymerase runoff reaction without GMPS. Each resulting RNA was purified using the procedures previously described.

***trans*-Phosphorothiolate Thiolesterase Assay.** The *trans*-phosphorothiolate thiolesterase reaction was conducted under multiple-substrate turnover conditions as follows: 300−900 nM internally ^{32}P-labeled S_{1-18} RNA−**4** conjugate and 30 nM $TW17_{22-87}$ ribozyme were folded independently and equilibrated with 20 mM $MgCl_2$ for 5 min. The reaction was initiated by the addition of Zn^{2+} (0.5 mM), with removal of a 10 μL aliquot from the 100 μL reaction mixture at specific times. Each reaction was quenched with 55 mM EDTA, and each mixture was precipitated twice with ethanol and analyzed by a SAv gel shift assay via 12% urea−PAGE or biphasic urea−PAGE (12% urea−PAGE for the top phase and 20% urea−PAGE for the bottom phase) and with an Amersham Typhoon PhosphorImager system. The initial velocity for each catalytic reaction in the presence of a specific concentration of the ^{32}P-labeled S_{1-18} RNA−**4** conjugate was obtained from linear regression analysis (Microsoft Excel) of the data from the first 3 h. The initial velocities and concentrations of the S_{1-18} RNA−**4** conjugate were performed using nonlinear analysis and fitting data to the Michaelis−Menten equation [$v = (V_{max}[S_{1-18}\ RNA])/(K_M + [S_{1-18}\ RNA])$], yielding K_M, k_{cat}, and k_{cat}/K_M (GraphPad).

The single-turnover *trans*-phosphorothiolate thiolesterase reaction was conducted as follows: 160 nM internally ^{32}P-labeled S_{1-18} RNA−**4** conjugate and 1.6 μM $TW17_{22-87}$ ribozyme were folded independently and equilibrated with 540 mM $MgCl_2$ for 5 min. The reaction was initiated by the addition of a Zn^{2+} solution (2.7 mM), followed by removal of a 10 μL aliquot from the 20 μL reaction mixture at a specified time over 96 h. Each reaction was quenched with 55 mM EDTA, and each mixture was precipitated twice with ethanol and analyzed by a SAv gel shift assay via 12% urea−PAGE and with an Amersham Typhoon PhosphorImager system.

Metal-Dependent Catalytic Activity. A survey of metal dependency for TW17 ribozyme catalysis was performed according to the same procedures for the general kinetic assays described above with the $ZnCl_2$ solution replaced with a divalent or monovalent metal chloride solution. Divalent (Ca^{2+}, Mn^{2+}, Co^{2+}, Cu^{2+}, Zn^{2+}, Ni^{2+}, and Cd^{2+}) and monovalent (Li^+) metal chloride solutions (10 mM) in DEPC water were freshly prepared. Each metal ion reaction mixture was aliquoted at time zero and after reaction for 3 h. The reaction products were separated by a SAv gel shift assay via 8% urea−PAGE and analyzed with an Amersham Typhoon PhosphorImager system.

RESULTS

Selection of a Phosphorothiolate Thiolesterase Ribozyme. The aim of the initial selection design was to simultaneously select three different ribozymes from a single in vitro selection in which each ribozyme catalyzed a specific Zn^{2+}-dependent reaction, including NADH-dependent disulfide reduction or amide or phosphorothiolate thiolester hydrolysis (Figure 1A). Before the initiation of ribozyme selection, we confirmed that the prepared RNA pool had no detectable ribozyme activity under the standard reaction conditions after incubation for 24 h (Figure S1C of the Supporting Information). Prior to round 14 of the selection, we adopted a less complicated selection strategy by pooling together the NADH-dependent and NADH-independent active sequences from each round while the reaction stringency was gradually increased. At round 14, we observed that a significant amount of RNA was eluted out of the SAv column before NADH incubation, an indication of extensively enriched RNA with NADH-independent activities. The RNA molecules, eluted before the NADH incubation, were pooled and subjected to six additional rounds of NADH-independent selection. At the end of the selection, a pool of RNA containing almost 8% of the total RNA was collected (Figure 1D). The selected RNA was subcloned; 50 clones were randomly chosen from that pool to study the NADH-independent activity. Two clones, TW17 and TW26, had RNA carrying the best and comparable activity in accordance with their essentially identical DNA sequences (Figure 1E). Only the TW17 ribozyme was further characterized because its NADH-independent activity was better than that of the TW26 ribozyme (Figure S1D of the Supporting Information).

The intriguing NADH-independent activity conferred by the TW17 ribozyme catalysis prompted us to scrutinize the requirement of the disulfide bond in **1** for the reaction. The nonessential role of NADH in TW17 ribozyme catalysis implied that reductive cleavage of the disulfide bond in **1** was apparently not involved in the TW17 ribozyme activity because reduction of the disulfide bond in **1** would require the assistance of a reductant such as NADH. We studied the specificity of the TW17 ribozyme upon reduction of the disulfide bond by conjugating the GMPS-primed TW17 ribozyme with substrates **1** and **4**, a structural analogue of **1** without the disulfide bond. The TW17 ribozyme demonstrated similar substrate specificity for either **1** or **4** (Figure S1E of the Supporting Information), and therefore, the TW17 ribozyme was not a disulfide reductase RNA. Substrate **4** was chosen for

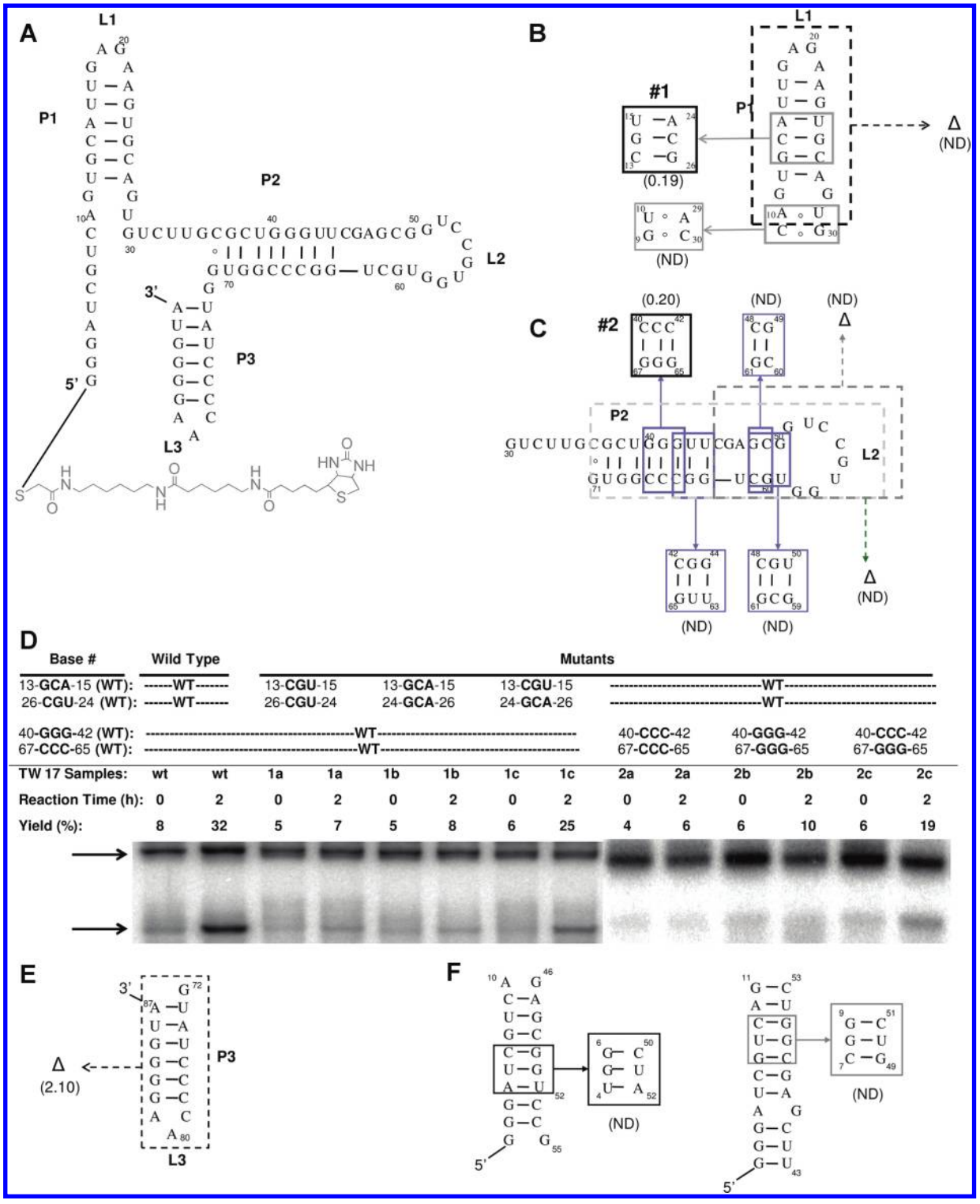

Figure 2. Determination of the secondary structure for the TW17 ribozyme when forming a conjugate with its substrate **4**. Twelve sets of mutants of the ribozyme were prepared by site-directed mutagenesis to explore the secondary structure of the TW17 ribozyme−**4** conjugate. (A) Determined secondary structure of the GMPS-primed TW17 ribozyme covalently linked to substrate **4** (gray). (B−F) In site-directed mutagenesis, each mutant underwent either sequence replacement (denoted by solid boxes and arrowa) or sequence deletion (denoted by dashed boxes and arrows) compared to the wild-type ribozyme. Only the TW17 ribozyme mutants with mutations at box 1 (B) and box 2 (C) and deletion at the 3′ end (E) demonstrated detectable activities. Relative activities compared to that of the wild-type ribozyme are shown in parentheses. Abbreviations: P, helix; L, loop; Δ, deletion mutation; ND, not detected. (D) The catalytic activities of box 1 and 2 mutants for the TW17 ribozyme were studied by a SAv gel shift assay via 10% urea−PAGE and analyzed with an Amersham Typhoon PhosphorImager system. The top arrow indicates the location of the nonreacted ^{32}P-labeled TW17 ribozyme−**4** conjugate; the bottom arrow denotes the migration of the ^{32}P-labeled TW17 ribozyme-catalyzed reaction product. (F) Site-directed mutagenesis studies indicate that the catalysis active form in the TW17 ribozyme did not have a pseudoknot secondary structure composed of the 5′ end and the L2 loop in the ribozyme.

dx.doi.org/10.1021/bi201585d | *Biochemistry* 2012, 51, 496−510

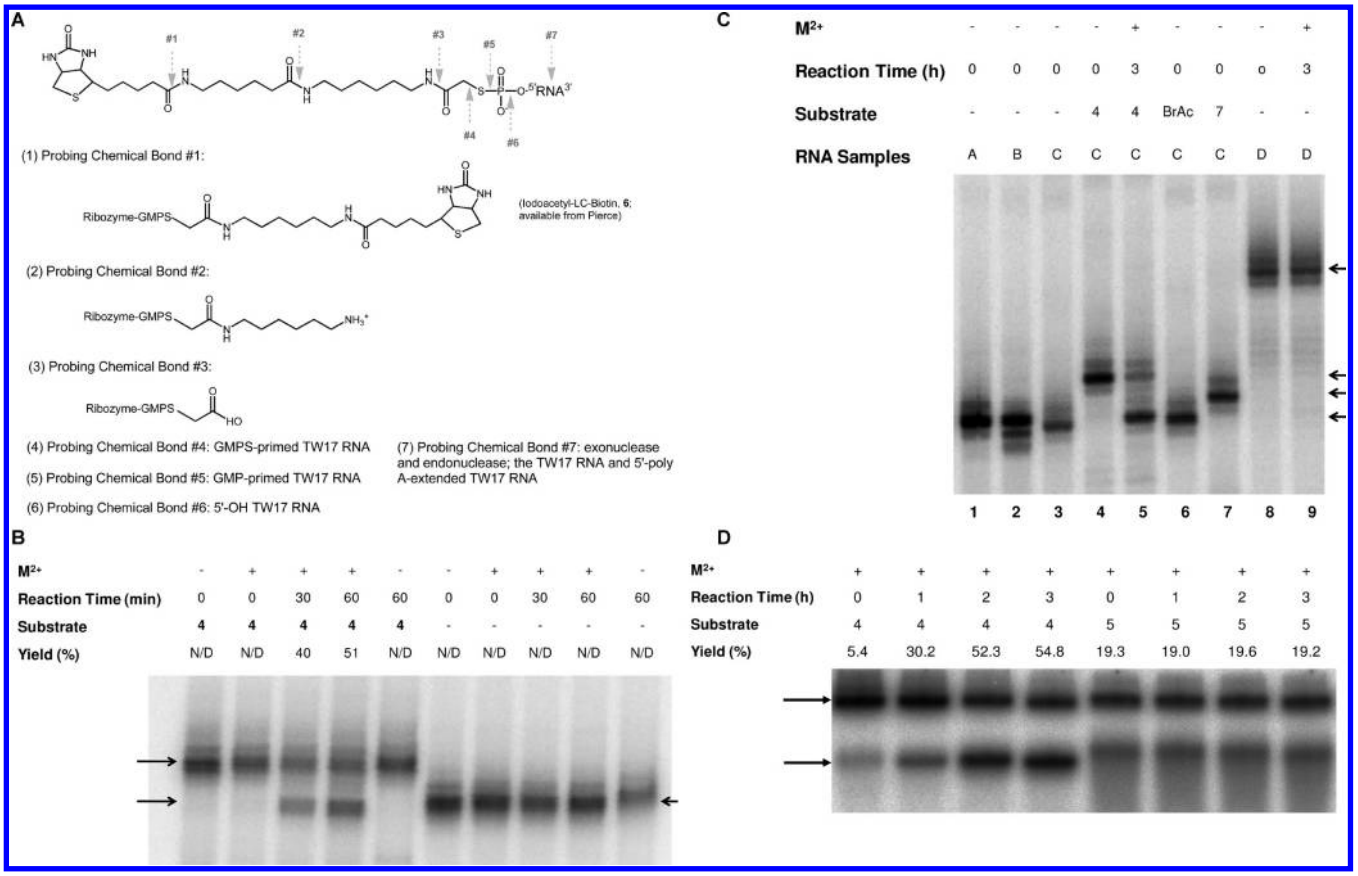

Figure 3. Analyzing the TW17 ribozyme reaction product to determine the substrate specificity and the catalytic mechanism of the TW17 ribozyme. (A) Possible enzymatic activity conferred by the TW17 ribozyme. Each arrow denoted with a number indicates a candidate reaction that might be catalyzed by TW17 ribozyme activity. Each arrow number has a corresponding number in parentheses to describe a TW17 ribozyme derivative that was used to study the potential of the ribozyme to catalyze hydrolysis of the specific chemical bond. See the text for details. (B) The TW17 ribozyme is not an endonuclease. The ^{32}P-labeled RNA samples were separated by high-resolution 10% sequencing urea−PAGE and analyzed with an Amersham Typhoon PhosphorImager system. The top arrow on the left indicates migration of the TW17 ribozyme−**4** conjugate; the bottom arrow on the left represents the location of the TW17 ribozyme reaction product; the arrow on the right denotes the mobility of the GMPS-primed TW17 ribozyme. (C) The TW17 ribozyme is not an exonuclease and is unable to catalyze hydrolysis of amide linkages in **4**. The ^{32}P-labeled RNA samples were separated by high-resolution 10% sequencing urea−PAGE and analyzed with an Amersham Typhoon PhosphorImager system. The RNA samples were as follows: (A) the GTP-primed TW17 ribozyme, (B) the GTP-primed TW17 ribozyme treated with alkaline phosphatase (Promega), (C) the GMPS-primed ribozyme, and (D) the GTP-primed 5′-poly-A-extended TW17 ribozyme. BrAc stands for bromoacetate. The four arrows on the right, from top to bottom, indicate migrations of the GTP-primed 5′-poly-A-extended TW17 ribozyme, the TW17 ribozyme−**4** conjugate, the TW17 ribozyme−**7** conjugate, and the TW17 ribozyme catalysis product, respectively. (D) The TW17 ribozyme is unable to catalyze hydrolysis of the TW17 ribozyme−**5** conjugate and thus is not an amidase RNA. The ^{32}P-labeled RNA−substrate conjugates were separated by a SAv gel shift assay via 8% urea−PAGE and analyzed with an Amersham Typhoon PhosphorImager system. The top arrow indicates the migration of the TW17 ribozyme−substrate conjugates retarded by SAv. The bottom arrow denotes the migration of the TW17 ribozyme catalysis product. In each graph, the addition of M^{2+} (+) indicates the presence of 100 mM Mg^{2+} and 0.5 mM Zn^{2+} in each reaction mixture.

the study of the kinetics and structure of the ribozyme because it could more easily be attained by organic synthesis and had better coupling efficiency when reacting with the GMPS-primed TW17 ribozyme (T.-P. Wang et al., unpublished results).

Secondary Structure of the TW17 Ribozyme. Plausible secondary structures for the TW17 ribozyme−**4** conjugate were evaluated with RNAstructure version 4.5.[27] A potential structure candidate with a low free energy (Figure S2A of the Supporting Information) was chosen as the model and led to the determination of the secondary structure of the TW17 ribozyme−**4** conjugate (Figure 2A). The site-directed mutagenesis studies provided the crucial evidence to support the determined secondary structure of the RNA conjugate (Figure 2B−E).

We prepared 12 sets of site-directed TW17 ribozyme mutants by either sequence replacements or deletions and studied correlations between structural changes and catalytic activity, especially the proposed local helix structures in the TW17 ribozyme (Figure S2A of the Supporting Information). The presence of a local helix structure in the TW17 ribozyme was demonstrated by the decrease in ribozyme activity when the base pairing within a proposed helix was disrupted and by the recovery of ribozyme activity when the base pairing within the helical region was restored through swapping of each RNA sequence in the helix. Only three of the 12 sets of the TW17 ribozyme mutants showed detectable catalytic activity. Two of the positive mutant sets for the TW17 ribozyme carried sequence permutations in box 1 in the P1 helix (Figure 2B) and box 2 in the P2 helix (Figure 2C). The loss of base pairing in box 1 or 2 completely abolished TW17 ribozyme activity

(mutants 1a, 1b, 2a, and 2b in Figure 2D). Mutants 1c and 2c, which had sequence exchanges but maintained base pairing in the proposed helices, reinstalled TW17 ribozyme activity, albeit with a lower catalytic efficiency than the wt ribozyme (Figure 2D). The kinetic study of the TW17 ribozyme mutants in boxes 1 and 2 clearly supported the integrity of helical structures in the two boxed areas as being indispensable for TW17 ribozyme catalysis. The local helix structure containing box 1 is composed of G13−A15 and U24−C26 in helix P1; the local helix structure consisting of G40−G42 and C65−C67 is a segment of helix P2 and contributes to box 2. We therefore concluded that helices P1 and P2 are present in the secondary structure for the catalysis-active form of the TW17 ribozyme. The third positive mutant has a sequence deletion at G72−A87 which encompasses the P3−L3 local structure in the wt TW17 ribozyme sequence (Figure 2E). The truncated mutant conducted better catalysis than the wt ribozyme (Figure S2B of the Supporting Information). Therefore, the P3−L3 local secondary structure in the wt TW17 ribozyme is an isolated system and not required for TW17 ribozyme catalysis.

Activity studies of the nine remaining sets of negative mutants for the TW17 ribozyme offered additional information about the secondary structure of the TW17 ribozyme−**4** conjugate. For example, the site-directed mutagenesis studies on the 5′ end of the TW17 ribozyme unveiled a relatively flexible local structure essential to catalysis after studies were not able to define a sturdy local helical structure for G1−U12. A similar scenario of a local dynamic structure comprised by C45−U62 (the L2 loop) was also required for TW17 ribozyme catalysis. The loss of ribozyme activity after deletion of A10−U29, C36−G71, or C45−U62 from the wt TW17 ribozyme again indicated the requirements of these nucleotides specifically located in the TW17 ribozyme structure for effective catalysis.

We were aware of the potential of the 5′ end G1−G11 segment to base pair with loop L2 to form a pseudoknot secondary structure in the TW17 ribozyme. Therefore, we prepared two sets of mutants, the A4−C6 segment−G50−U52 segment pair and the G7−C9 segment−C49−G51 segment pair, and studied changes in catalysis activity after site-directed mutagenesis in each set (Figure 2F). None of the mutants showed detectable activity, ruling out the presence of a pseudoknot secondary structure in the catalysis-active form of the TW17 ribozyme. Overall, the results from the site-directed mutagenesis studies on the TW17 ribozyme−**4** conjugate were compliant with the determined three-helix secondary structure for the ribozyme that consisted of three major helices [P1−P3 (Figure 2A)] and three loops [L1−L3 (Figure 2A)].

Product Analysis. First, we tackled the challenge of demonstrating that the TW17 ribozyme indeed catalyzes a new chemical reaction not previously reported for ribozyme catalysis. We had already precluded the possibility that the TW17 ribozyme was a disulfide reductase RNA according to the equivalent catalysis ability in the TW17 ribozyme when conjugated with **1** or **4** (Figure S1E of the Supporting Information). However, the TW17 ribozyme−**4** conjugate carried various functional groups and likely different local structures that could be recognized by the catalytic center in the ribozyme to confer the observed activity and the presumed substrate specificity (Figure 3A). The presence of multiple functional groups in **4**, the phosphorothiolate thiolester bond between **4** and the TW17 ribozyme, and various phosphodiester linkages in the TW17 ribozyme complicated efforts to unambiguously determine the type of chemical reaction catalyzed by the TW17 ribozyme and to identify the reaction products of TW17 ribozyme catalysis. We carefully performed systematic analysis of TW17 ribozyme catalysis reactions to unambiguously determine the substrate specificity and the chemical identity of the reaction catalyzed by the ribozyme (vide infra).

We first demonstrated that the TW17 ribozyme was not an endonuclease RNA. The TW17 ribozyme had no detectable catalytic ability when substrate **4** was not conjugated to the ribozyme before the catalytic reaction (Figure 3B). We further ruled out the possibility that the TW17 ribozyme could be an exonuclease by studying a TW17 ribozyme mutant with a 5′-GAA AAA AAA AA-3′ sequence appended to its 5′ end (the 5′-poly-A-extended TW17 ribozyme) and subsequently conjugated with **4** with quantitative yields (T.-P. Wang et al., unpublished results). The 5′-poly-A-extended TW17 ribozyme showed no detectable catalytic activity after a 3 h reaction, which suggested that the TW17 ribozyme was not an exonuclease RNA (Figure 3C, lanes 8 and 9). However, we could not exclude the possibility that the loss of **4** or appending a poly-A tail to the 5′ end of the TW17 ribozyme might change the conformation of the ribozyme and transform it into a catalysis-inactive form.

We addressed the lingering question of the likelihood of nuclease activity conferred by TW17 ribozyme catalysis. We performed an atom replacement assay to study changes in TW17 ribozyme catalysis after substituting a phosphoramidate bond (between the RNA and substrate **5**) for the phosphorothiolate thiolester linkage (between the RNA and **4**) in the RNA conjugates. We previously reported synthesis of **5** and effectively conjugated the compound to GMP-primed RNA by a one-step phosphoramidation reaction.[25] We reasoned that the replacement of S (covalent radius of 103 pm) with N (covalent radius of 75 pm) in the TW17 ribozyme−substrate conjugates was a minor change in the structure of the RNA conjugate and was thus less likely to induce a global difference in conformation to cause a reduction or loss of catalytic activity in the TW17 ribozyme. In contrast to the TW17 ribozyme−**4** conjugate, the TW17 ribozyme−**5** conjugate did not exhibit any traces of catalytic activity (Figure 3D). The loss of catalytic activity in the TW17 ribozyme−**5** conjugate, therefore, could not be attributed to a failure of the conjugate to fold into a catalysis-active conformation to cause the loss of activity in the ribozyme. The results strongly supported the inability of the TW17 ribozyme to be endonuclease or exonuclease RNA. Moreover, a complete loss of catalytic activity in the TW17 ribozyme−**5** conjugate implied that the TW17 ribozyme might have catalytic specificity in the hydrolysis of the phosphorothiolate thiolester linkage between the ribozyme and substrate **4**, rather than in the hydrolysis of one or more of the three amide bonds in **4**. In addition, the TW17 ribozyme catalysis product and the 5′-OH TW17 ribozyme had a distinguishable migration difference as determined by high-resolution PAGE, supporting the idea that the ribozyme did not catalyze hydrolysis of the phosphoester (P−O) linkage between the RNA and the phosphate next to **4** (Figure S3A of the Supporting Information).

We provided additional support for the idea that the TW17 ribozyme was a phosphorothiolate thiolesterase RNA by demonstrating that two of the three amide linkages in **4** were not hydrolyzed by the TW17 ribozyme. First, we showed that the amide bond directly adjacent to the biotin moiety in **4** was

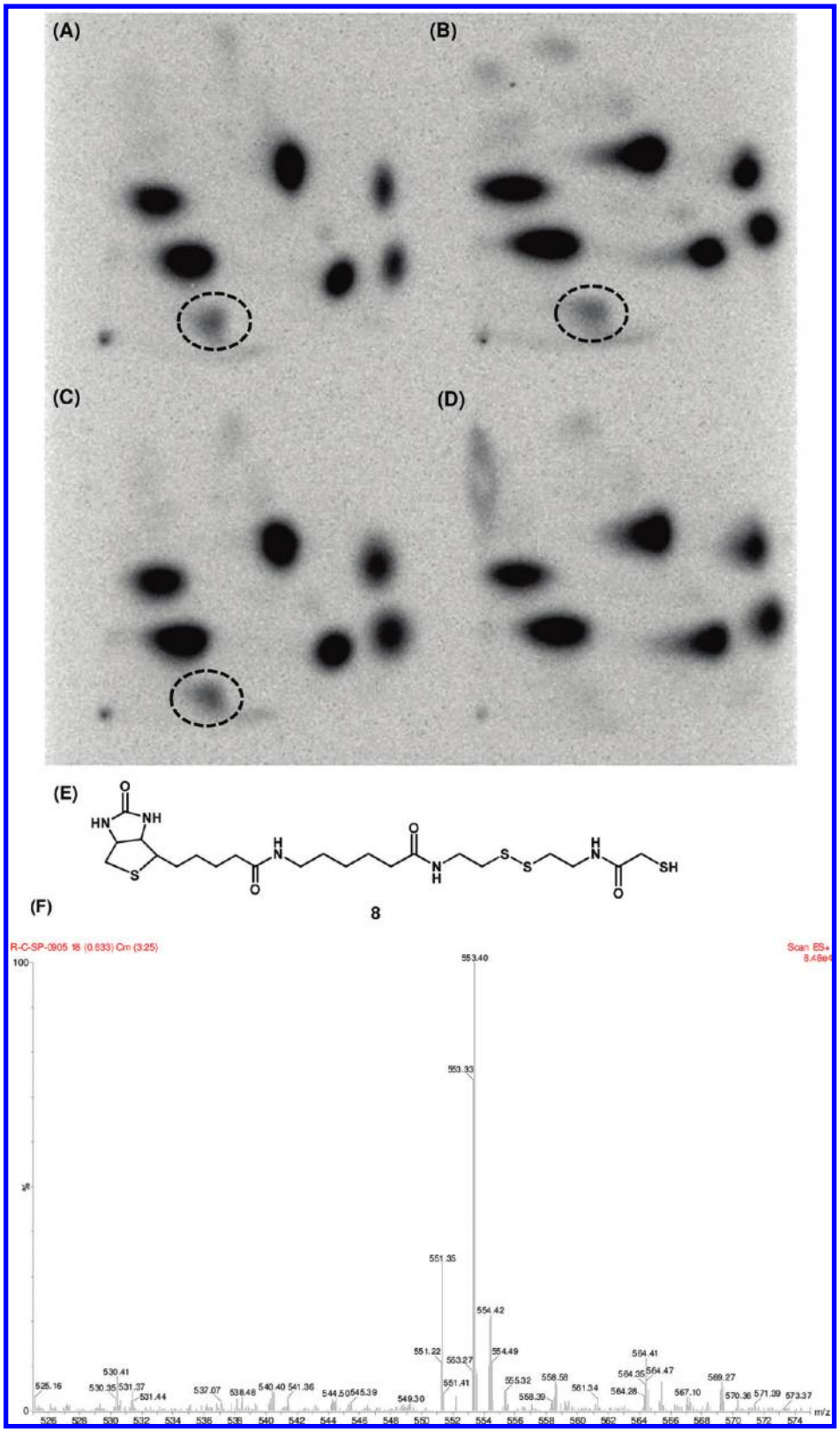

Figure 4. Two-dimensional TLC and ESI-MS analyses to demonstrate the TW17 ribozyme as phosphorothiolate thiolesterase RNA. The ^{32}P-labeled samples of (A) the purified TW17 ribozyme catalysis product, (B) the GMP-primed TW17 ribozyme, (C) an equal mixture of samples A and B, and (D) the TW17 ribozyme−**4** conjugate were subjected to RNase T2 digestion and followed by 2D TLC analysis. Refer to the text for details of RNase T2 digestion and 2D TLC analysis. The results were visualized with an Amersham Typhoon PhosphorImager system. The characteristic reaction product from the TW17 ribozyme catalysis (pGp) is circled. (E) Molecular structure of **8**, which is one of the ribozyme-catalyzed reaction products. (F) ESI-MS spectrum to confirm the identity of **8**. The signal at m/z 553.40 corresponds to the expected mass of **8** ($[M + Na]^+$).

dx.doi.org/10.1021/bi201585d | *Biochemistry* 2012, 51, 496−510

not the linkage hydrolyzed during TW17 ribozyme catalysis as the TW17 ribozyme maintained excellent catalytic activity when the ribozyme formed a conjugate with substrate **6** (Figure S3B of the Supporting Information). The major structural difference between **4** and **6** was the closest amide linkage to the biotin moiety in **4** (Figure 1C). The middle amide bond in **4** was ruled out as the linkage hydrolyzed by TW17 ribozyme catalysis when high-resolution urea−PAGE analysis demonstrated a significant difference in mobility between the TW17 ribozyme catalysis products and the TW17 ribozyme−**7** conjugate (Figure 3C, lanes 5 and 7). However, we could not clearly distinguish the difference in migration between the TW17 ribozyme catalysis product and the TW17 ribozyme−bromoacetate conjugate (Figure 3C, lanes 5 and 6). In addition, the high-resolution urea−PAGE analysis also could not unequivocally resolve the difference in migration between the GMPS-primed TW17 ribozyme and the TW17 ribozyme catalysis product (Figure 3C, lanes 3 and 5). We addressed the latter question by purifying the TW17 ribozyme catalysis product and analyzing it with APM−PAGE and urea−PAGE. The results clearly indicated that the TW17 ribozyme catalysis product was not a GMPS-primed RNA because RNA mobility was not retarded in APM−PAGE (Figure S3C of the Supporting Information). We, however, could not completely eliminate the possibility that the TW17 ribozyme was an amidase RNA and catalyzed the hydrolysis of the amide bond directly adjacent to the RNA.

Two-dimensional TLC analysis provided convincing evidence supporting the idea that the TW17 ribozyme is specific to the catalysis of phosphorothiolate thiolester hydrolysis with no catalytic activity toward the closest amide bond to the TW17 ribozyme (Figure 4A−D and Figure S4A−D of the Supporting Information). The RNase T2-digested TW17 ribozyme reaction product and the TW17 ribozyme−bromoacetate conjugate exhibited a distinguishable difference in their migration patterns after 2D TLC analysis (Figure S4C,D of the Supporting Information), ruling out the possibility of the TW17 ribozyme as an amidase RNA. The same 2D TLC analysis also indicated that the RNase T2-digested TW17 ribozyme reaction product produced results very similar to those of the RNase T2-digested GMPS-primed and GMP-primed TW17 ribozymes. A previous result had already demonstrated that the TW17 ribozyme catalysis product was not a GMPS-primed RNA (Figure S3C of the Supporting Information). Therefore, the TW17 ribozyme catalysis product was a GMP-primed RNA that was further supported by a second 2D TLC analysis (Figure 4A−D). The RNase T2-digested TW17 ribozyme reaction product and the GMP-primed TW17 ribozyme again showed an identical result after 2D TLC analysis (Figure 4A,B). A very similar result was obtained when the purified TW17 ribozyme reaction product and the GMP-primed TW17 ribozyme were mixed together, digested with RNase T2, and analyzed by 2D TLC (Figure 4C). The identified characteristic reaction product pGp,[28] circled in Figure 4, was clearly not present in the TW17 ribozyme−**4** conjugate or the TW17 ribozyme−bromoacetate conjugate both was subjected to RNase T2 digestion and 2D TLC analysis (Figure 4D and Figure S4D of the Supporting Information).

Finally, mass spectrometry offered direct evidence that the TW17 ribozyme is a phosphorothiolate thiolesterase RNA. ESI-MS analysis of the biotin-containing reaction product from *cis*-acting catalysis showed a major signal at m/z 553.40 that corresponded to the expected mass ($[M + Na]^+$) of biotin-containing compound **8** when the phosphorothiolate thiolester bond was hydrolyzed (Figure 4E,F). The identification of **8** clearly supports the conclusion of the TW17 ribozyme is a phosphorothiolate thiolesterase RNA. In summary, results from biochemical and chemical analyses of the ribozyme-catalyzed reaction products were consistent with the conclusion that the TW17 ribozyme is a phosphorothiolate thiolesterase RNA in which the GMP-primed TW17 ribozyme and **8** were the products of ribozyme catalysis.

Kinetics. The time course study for TW17 ribozyme catalysis indicated that 50−60% of the products were formed after reaction for 3 h (Figure 5A). Longer reaction times did not significantly improve product yields for TW17 ribozyme catalysis in which the catalysis-inactive TW17 ribozyme conformation constituted 40−50% of the total population and was stable enough to persist throughout the reaction time (T.-P. Wang et al., unpublished result). We currently have no evidence to support an explanation for the kinetic behavior of the ribozyme. We calculated the percent RNA cleavage at each

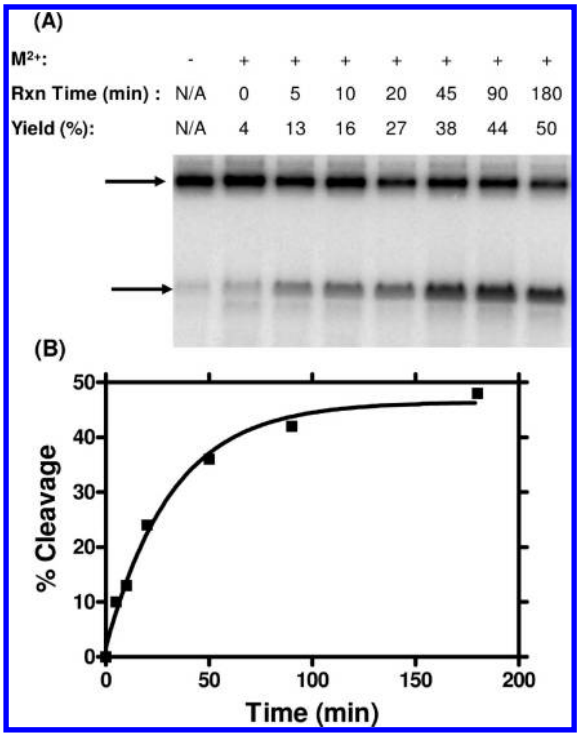

Figure 5. Kinetics of the chemical reaction catalyzed by the TW17 ribozyme. (A) Time course study of catalysis for the ^{32}P-labeled GMPS-primed TW17 ribozyme previously conjugated with **4**. The concentrations of metal ions (M^{2+}), if used, were 100 mM Mg^{2+} and 0.5 mM Zn^{2+} in the TW17 ribozyme catalysis. The reaction products from each time point were separated by a SAv gel shift assay via 8% urea−PAGE and analyzed with an Amersham Typhoon Phosphor-Imager system. The top arrow indicates the location of the SAv-retarded ^{32}P-labeled TW17 ribozyme−**4** conjugate; the bottom arrow denotes the migration of the ^{32}P-labeled TW17 ribozyme-catalyzed reaction product. (B) Determination of the pseudo-first-order rate constant (k_{obs}) for TW17 ribozyme catalysis under standard reaction conditions. Data obtained from ImageQuant analysis in panel A were fitted to a single-exponential equation for first-order kinetics [$F(t) = F_0 + F_{max}(1 - e^{-k_{obs}t})$, where $F(t)$ is the percent cleavage of the reactant at time t (GraphPad)] to afford a pseudo-first-order rate constant (k_{obs}) of 0.028 min^{-1} for TW17 ribozyme catalysis.

dx.doi.org/10.1021/bi201585d | *Biochemistry* 2012, 51, 496−510

time point and performed nonlinear curve fitting on the data to acquire a pseudo-first-order rate constant (k_{obs}) of 0.028 min^{-1} at 25 °C for TW17 ribozyme catalysis (Figure 5B). Because the original RNA pool showed no appreciable catalytic activity after a 24 h background reaction (Figure S1C of the Supporting Information), catalysis of the TW17 ribozyme presented a rate enhancement of at least 5 orders of magnitude when compared to the slower estimated rate of the uncatalyzed reaction, 7×10^{-8} min^{-1}.[12] The TW17 ribozyme is an excellent RNA enzyme catalyzing phosphorothiolate thiolester hydrolysis.

***trans*-Phosphorothiolate Thiolesterase Activity.** The original design of the selection scheme confined the TW17 ribozyme to evolve and be selected as a *cis*-acting catalyst that prohibited multiple-turnover catalysis. However, a hallmark of modern protein enzymes is to effectively catalyze multiple substrate turnovers in addition to using their unique catalysis mechanisms. Therefore, the TW17 ribozyme was reconstructed to mimic multiple-substrate turnover catalysis performed by protein enzymes and to support their plausible metabolic functions in primordial life. Construction of an *in trans* ribozyme catalysis system in vitro is often achieved by dissecting the *cis*-acting ribozyme into a substrate-bearing nucleotide sequence and a major catalytic core RNA based on the previously determined secondary structure for a ribozyme.[8,11,29−32] The wt TW17 ribozyme structure was thus divided into two segments by removing three nucleotides in loop L1 to discontinue the wt ribozyme that transformed it into a *trans*-acting catalysis system (Figure 6A). A valid *trans*-acting ribozyme catalysis system derived from the wt TW17 ribozyme would support the determined secondary structure for the ribozyme and demonstrate potential of the ribozyme to convey multiple-substrate turnover catalysis (Figure 2A).

The constructed *in trans* catalysis system of the TW17 ribozyme successfully catalyzed the expected chemical transformation under the standard reaction condition, albeit at an efficiency lower than that of the *cis*-acting wt TW17 ribozyme (Figures 5 and 6 and Figure S5 of the Supporting Information). We initially intended to improve the product yields of the ribozyme catalysis system for subsequent analysis by adopting the potential of the *trans*-acting TW17 ribozyme catalysis system to perform single-substrate turnover and attain maximal catalysis. Unexpectedly, the *trans*-acting TW17 ribozyme catalysis system still only provided an 18% product yield even after reaction for 96 h under the single-substrate turnover condition (Figure S5A of the Supporting Information). In addition, the *trans*-acting catalysis system is analogous to the *cis*-acting wt TW17 ribozyme that reached its maximal product yield after reaction for 3 h (Figures 5A and 6B and Figure S5B of the Supporting Information). The k_{obs} of the *trans*-acting catalysis system is 0.0059 min^{-1}, which is only one-fifth of the value of the *cis*-acting ribozyme (Figure S5C of the Supporting Information). We again purified the biotin-containing catalysis product of the *trans*-acting TW17 ribozyme system and demonstrated the molecular ion signal corresponding to **8** by ESI-MS analysis (Figure S5D of the Supporting Information). The similarity implied that both ribozymes might share a common catalytic mechanism and identical catalytic characteristics such as substrate specificity.

The *trans*-acting TW17 ribozyme catalysis system, however, exhibited only marginal multiple-substrate turnover ability. We measured the initial velocity of the *trans*-acting TW17 ribozyme catalysis system for the TW17 ribozyme at varied concentrations of the substrate RNA (S_{1-18} RNA, 300−900 nM), a constant ribozyme ($TW17_{22-87}$ ribozyme) concentration (30 nM), and a constant excess of substrate (Figure S5F of the Supporting Information). Nonlinear curve fitting of the data of initial velocity, versus a substrate concentration, to the Michaelis−Menten equation allowed the acquisition of essential kinetic parameters for the *in trans* TW17 ribozyme catalysis system: K_M = 1.77 ± 1.20 μM, k_{cat} = 1.65 ± 0.80 min^{-1}, and k_{cat}/K_M = (1.6 ± 1.3) × 10^4 s^{-1} M^{-1} (Figure S5F of the Supporting Information). The second-order rate constant k_{cat} indicates that the *trans*-acting ribozyme system at best catalyzed two substrate turnovers per minute. Nevertheless, the success in demonstrating that the constructed *in trans* TW17 ribozyme system performs the desired catalysis provides additional

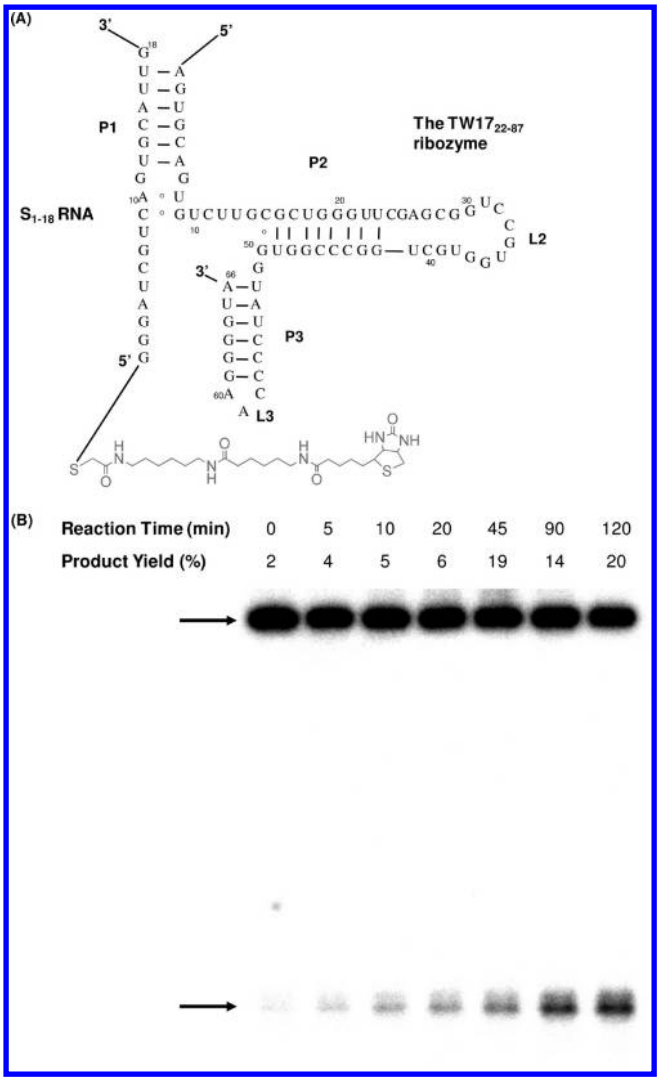

Figure 6. Structure and catalysis of a *trans*-acting TW17 ribozyme system. (A) Structural design for the *trans*-acting TW17 ribozyme system. Please see Materials and Methods for the preparation of the S_{1-18} RNA and the mini catalytic $TW17_{22-87}$ ribozyme. (B) Catalysis of the *in trans* TW17 ribozyme catalysis system containing 30 nM mini catalytic $TW17_{22-87}$ ribozyme and 300 nM ^{32}P-labeled S_{1-18} RNA−**4** conjugate, which is a multiple-substrate turnover condition. Reaction products were separated by a SAv gel shift assay via 12% urea−PAGE and analyzed with an Amersham Typhoon PhosphorImager system. The top arrow in the figure indicates the location of the SAv-retarded ^{32}P-labeled S_{1-18} RNA−**4** conjugate; the bottom arrow denotes the migration of the ^{32}P-labeled GMP-primed S_{1-18} RNA produced by TW17 ribozyme catalysis.

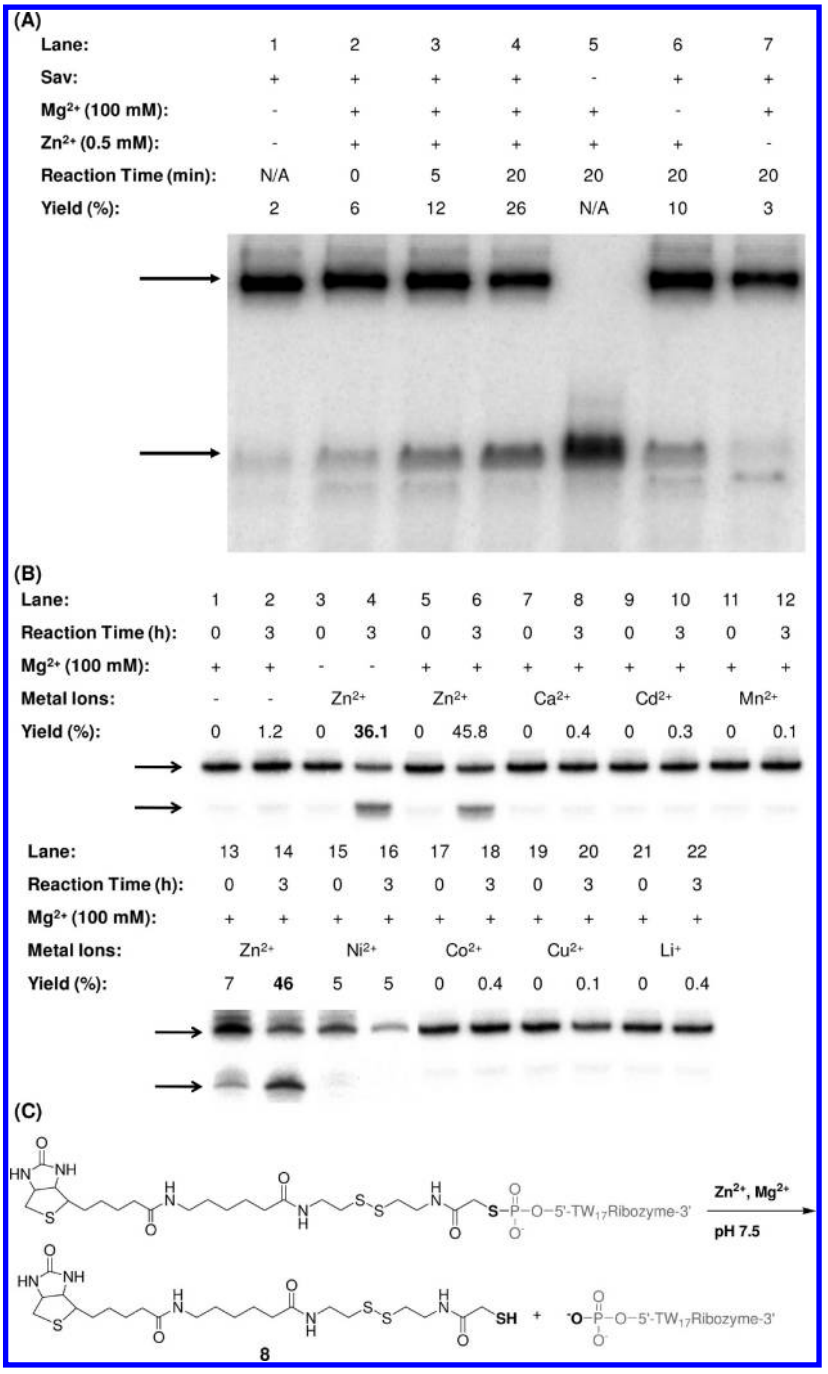

Figure 7. Absolute requirement of Zn^{2+} for TW17 ribozyme catalysis. (A) Zn^{2+} alone is sufficient for TW17 ribozyme catalysis. The ^{32}P-body-labeled GMPS-primed TW17 RNA previously conjugated with **4** catalyzed each reaction under the preset conditions. The concentrations of metal ions, when provided, were 100 mM Mg^{2+} and 0.5 mM Zn^{2+}. Reaction products were also separated by a SAv gel shift assay via 8% urea−PAGE and analyzed with an Amersham Typhoon PhosphorImager system. The top arrow in the figure indicates the location of the SAv-retarded ^{32}P-labeled TW17 ribozyme−**4** conjugate; the bottom arrow denotes the migration of the ^{32}P-labeled TW17 ribozyme-catalyzed reaction product except for lane 5, for which it denotes the location of the non-SAv-bound TW17 ribozyme. (B) Profiling studies for the metal ion dependency of TW17 ribozyme catalysis. The ^{32}P-body-labeled GMPS-primed TW17 RNA previously conjugated with **4** underwent catalytic reactions under each specified condition. Metal concentrations in each reaction were 0.5 mM except 100 mM for Mg^{2+}. Reaction products were also separated by a SAv gel shift assay via 8% urea−PAGE and analyzed with an Amersham Typhoon PhosphorImager system. The top arrow in the figure indicates the location of the SAv-retarded ^{32}P-labeled TW17 ribozyme−**4** conjugate; the bottom arrow denotes the migration of the ^{32}P-labeled TW17 ribozyme-catalyzed reaction product. (C) Reaction scheme catalyzed by the TW17 ribozyme activity.

support for the determined secondary structure of the ribozyme shown in Figure 2A. The accurate secondary structure for the TW17 ribozyme can lead to the design of more catalysis-efficient and truly multiple-substrate turnover *trans*-acting systems for the ribozyme.

Absolute Requirement of Zn^{2+} Ions for TW17 Ribozyme Catalysis. The TW17 ribozyme is unusual among catalytic RNA molecules because the catalytic ability is dramatically weakened in the absence of Zn^{2+} ion (Figure 7A). The sole presence of Zn^{2+} ion was enough to support

dx.doi.org/10.1021/bi201585d | *Biochemistry* 2012, 51, 496−510

TW17 ribozyme catalysis even though that the percent yield of Zn^{2+} only catalysis was 20% of that of TW17 ribozyme catalysis in the presence of Zn^{2+} and Mg^{2+}. In parallel, the determined k_{obs} for the Zn^{2+}-only TW17 ribozyme catalysis reaction under the standard condition was only 0.005 min^{-1} (Y. Chen and T.-P. Wang, unpublished results), which is 18% of the k_{obs} for TW17 ribozyme catalysis in the presence of Zn^{2+} and Mg^{2+} (Figure 5B). In essence, the TW17 ribozyme is a metalloenzyme analogous to protein hydrolases with similar Zn^{2+} requirements.[33] The absolute Zn^{2+} dependency of TW17 ribozyme catalysis is intriguing and different from that of a Zn^{2+}-dependent aldolase ribozyme, which confers only 6% of its maximal activity in a Zn^{2+}-only catalytic reaction.[11] In addition to Zn^{2+} dependency, the TW17 ribozyme exhibited better catalytic activity upon addition of Mg^{2+} (Figure 7A). Although the presence of Mg^{2+} was not absolutely required for catalysis, the addition of Mg^{2+} promoted the TW17 ribozyme to achieve maximal catalysis. Mg^{2+} is unlikely to directly participate in TW17 ribozyme catalysis but may be essential in assisting the TW17 ribozyme to fold into an active conformation crucial to ribozyme catalysis.

We further explored the influence of other metal ions on TW17 ribozyme catalysis to provide insight into the intricate role of Zn^{2+} in the hydrolysis reaction. Previous studies of substitutions of active site Zn^{2+} with other metal ions similar in size and charge such as Co^{2+}, Mn^{2+}, and Cd^{2+} have shown the substitutions restore the catalytic activity of thermolysin.[34] However, none of the metal ions studied, including Co^{2+}, a close chemical analogue to Zn^{2+}, were able to substitute for Zn^{2+} to support TW17 ribozyme catalysis in the presence of Mg^{2+} (Figure 7B). These results again demonstrated the unique and indispensable role of Zn^{2+} in TW17 ribozyme catalysis. We concluded that the TW17 ribozyme was a phosphorothiolate thiolesterase RNA for which the GMP-primed TW17 ribozyme and **8** are the products after ribozyme catalysis in the presence of Zn^{2+} (Figure 7C).

DISCUSSION

We successfully identified the TW17 ribozyme from an artificial RNA pool and extensively characterized the catalytic reaction of the ribozyme. The TW17 ribozyme performed good catalytic activity for the hydrolysis of a phosphorothiolate thiolester bond in the presence of Zn^{2+} (Figures 5 and 7). The secondary structure for the 87-nt TW17 ribozyme was determined by site-directed mutagenesis and further studied by a *trans*-acting TW17 ribozyme catalysis system (Figures 2 and 6). The absolute requirement of Zn^{2+} for TW17 ribozyme catalysis together with the incorporation of Zn^{2+} and Mg^{2+} to achieve maximal reaction rates indicated a unique catalytic mechanism for the TW17 ribozyme among known ribozyme mechanisms (Figures 5 and 7). Identification and characterization of the TW17 ribozyme provide an opportunity to study an intriguing Zn^{2+}-dependent catalytic mechanism and the possible unique role of Zn^{2+} in RNA-based metabolic systems during primordial life.

A survey of major databases provided a dearth of knowledge about protein enzymes able to hydrolyze a phosphorothiolate thiolester linkage. The presence of a phosphorothiolate thiolesterase protein enzyme in nature remains plausible but requires additional effort to identify such an enzyme because of the uncertainty of phosphorothiolate thiolester linkages in biological systems. Yet from a chemistry perspective, phosphorothiolate thiolester bonds are functional analogues of phosphoester or carboxyl thiolester bonds. There are many Zn^{2+}-dependent phosphoesterases (e.g., teichoic acid phosphorylcholine esterase, methyl parathion hydrolase, Class II 3′,5′-cyclic nucleotide phosphodiesterase, phosphotriesterase, and phosphatase) and carboxyl thiolesterases (e.g., such as glyoxalase II) in modern protein-based living organisms.[16,33] These protein enzymes are embraced by a massive group of Zn^{2+}-dependent enzymes, zinc hydrolases.[33,35] Zinc plays a crucial role in expediting hydrolysis of the chemical bonds in these protein enzymes. The discovered TW17 ribozyme thus belongs to an expanding zinc hydrolase superfamily requiring Zn^{2+} for specific catalysis.

A similar absolute requirement of Zn^{2+} for catalysis has also been observed on a ribozyme for the Zn^{2+}-dependent aldol reaction.[11] The aldolase ribozyme also demands the assistance of Mg^{2+} to attain maximal catalysis. Other transition metal ions such as Co^{2+}, Ni^{2+}, and Cd^{2+} cannot substitute for Zn^{2+} in conferring the aldolase ribozyme activity. These parallel properties suggest that both ribozymes could share a similar catalytic mechanism in which Zn^{2+} plays an essential role to achieve the desired rate-enhancing reactions. However, the size (194-nt) and the secondary structure for the aldolase ribozyme are drastically different from those of the TW17 ribozyme. Moreover, there have been no detailed reports about the structure to catalysis correlation of the aldolase ribozyme to improve our understanding of its catalytic mechanism.

We have studied the catalytic mechanism for the TW17 ribozyme by experiments including pH and metal titrations. Our results indicate that the TW17 ribozyme uses the Zn^{2+} ions as a general base to promote the ribozyme catalysis while the Mg^{2+} ions, especially the outer-sphere Mg^{2+} ions, assist the ribozyme to fold into a catalysis-active conformation (Y. Chen and T.-P. Wang, unpublished results). The identified function of Zn^{2+} in the TW17 ribozyme catalysis is consistent with properties of zinc hydrolases in which zinc expedites hydrolysis reactions through its crucial role of performing general acid or base catalysis, or facile ligand replacement.[17,35,36] Detailed accounts of the mechanisms of TW17 ribozyme catalysis will be published in the future.

The structure−activity relationship studies for the TW17 ribozyme conjugated with **4** or **6** (Figure 5A and Figure S3B of the Supporting Information) suggested that the distance between the TW17 ribozyme and its biotin moiety was not critical to ribozyme catalysis. Moreover, it is possible that the TW17 ribozyme exploits not only its L2 loop to recognize the biotin portion in the substrate but also a metastable structure in helix P1 to properly align the phosphorothiolate thiolester with the ribozyme active site. The dynamic structural characteristics of helix P1 and loop L2 in the ribozyme have been indicated by the results of site-directed mutagenesis (Figure 2). However, the secondary structure of helix P2 and loop L2 in the TW17 ribozyme is very different from a known biotin-binding pseudoknot in a self-alkylating ribozyme.[8,37] Therefore, the structure argues against the helix P2−loop L2 structure in the TW17 ribozyme as a biotin-binding aptamer motif capable of recognizing biotin. Other possibilities include the presence of biotin-binding aptamers with structures similar to helix P2 of the ribozyme but not yet discovered or biotin recognition by the TW17 ribozyme not required for attaining the observed catalysis. We presently favor a mechanism in which the TW17 ribozyme uses its L2 loop to recognize the substrate and sets the stage for the phosphorothiolate thiolester linkage adsorbed on the catalytic center of the ribozyme in which interactions are

significantly enhanced by a relatively flexible P1 helix of the ribozyme. Studies to distinguish the possible process for substrate recognition by the ribozyme to attain a rather broad substrate specificity are in progress.

The structural flexibility of helix P1 in the TW17 ribozyme can be one of the major factors contributing to limited multiple-turnover catalysis performed by the *trans*-acting TW17 ribozyme system. In the *in trans* catalysis system, the mini catalytic $TW17_{22-87}$ ribozyme relied primarily on re-formation of helix P1 that was facilitated by adsorption of the substrate-bearing S_{1-18} RNA to the mini ribozyme to salvage phosphorothiolate thiolester hydrolysis activity. The metastable re-formed P1 helix is a guarantee of the continuous entrance of the substrate and departure of the products. The observed marginal multiple-turnover catalysis for the mini catalytic $TW17_{22-87}$ ribozyme reflects imbalance between regeneration of helix P1 and "breathing" of helix P1 to allow product dissociations that contribute to the poor value of k_{cat}.

The importance of loop L1 in effective ribozyme catalysis was manifested when the *trans*-acting TW17 ribozyme system delivered only ~20% of the efficiency of *cis*-acting ribozyme catalysis under single-substrate turnover conditions (Figures 2A, 4B, and 6A and Figure S5C of the Supporting Information). Indeed, the GAGA sequence of the L1 loop belongs to the family of GNRA tetraloops that are frequently involved in long-range RNA tertiary interactions.[38] Loop L1 in the wt TW17 ribozyme thus may interact with the helix P2–loop L2 local structure to stabilize the active conformation essential to ribozyme catalysis. Similarly, possibly suboptimal interaction of the GAGA sequence of loop L1 and the helix P2–loop L2 local structure may not be enough to stabilize the active conformation of the wt TW17 ribozyme and may contribute to at most 60% product conversion after prolonged catalysis by the wt ribozyme (Figure 5B). We are again studying structure–activity correlations of wt TW17 ribozyme catalysis by replacing the GAGA sequence of loop L1 with non-GNRA (such as UUCG) or other GNRA tetraloops to determine the functions of loop L1 in TW17 ribozyme catalysis. We also have already designed and studied several different *trans*-acting ribozyme systems by retaining loop L1 and changing the number of Watson–Crick base pairs in regenerated helix P1. Our goal was to decrease K_M, to increase k_{cat}, and to improve multiple-turnover catalysis in the *trans*-acting TW17 ribozyme catalysis system simultaneously.

In summary, our extensive structural characterization and catalytic reaction studies of the TW17 ribozyme pave the way for understanding fundamental chemistry harnessed by Zn^{2+}-dependent ribozymes. Continuous efforts to discover other Zn^{2+}-dependent ribozymes to encompass all six IUB classes of enzymatic reactions will further reveal the essential function of Zn^{2+} in life and may have implications on explicating the proposed process of the evolution of life progressing from an RNA world.

■ ASSOCIATED CONTENT

Supporting Information

Five extensive figures and one table. This material is available free of charge via the Internet at http://pubs.acs.org.

■ AUTHOR INFORMATION

Corresponding Author

*Department of Medicinal and Applied Chemistry, Kaohsiung Medical University, Kaohsiung 80708, Taiwan. E-mail: tzupinw@cc.kmu.edu.tw. Telephone: +886-07-312-1101, ext. 2756. Fax: +886-07-312-5339.

Funding

This work was supported by the National Science Council of Taiwan (Grants NSC95-2113-M-037-007/008, NSC96-2113-M-037-004-MY2, and NSC99-2113-M-037-008 to T.-P.W.).

■ ACKNOWLEDGMENTS

We thank Dr. Hiroaki Suga for his generous support of the initial phase of this research. We also gratefully acknowledge Dr. Huey-Nan Wu for sharing her expertise in deciphering the TW17 ribozyme secondary structures. We finally thank Drs. Susan Fetzer and Huey-Nan Wu for critical reading and helpful discussion of the manuscript.

■ REFERENCES

(1) Guerrier-Takada, C., Gardiner, K., Marsh, T., Pace, N., and Altman, S. (1983) The RNA moiety of ribonuclease P is the catalytic subunit of the enzyme. *Cell 35*, 849–857.

(2) Kruger, K., Grabowski, P. J., Zaug, A. J., Sands, J., Gottschling, D. E., and Cech, T. R. (1982) Self-splicing RNA: Autoexcision and autocyclization of the ribosomal RNA intervening sequence of *Tetrahymena*. *Cell 31*, 147–157.

(3) Gilbert, W. (1986) Origin of Life: The RNA World. *Nature 319*, 618.

(4) Chen, X., Li, N., and Ellington, A. D. (2007) Ribozyme catalysis of metabolism in the RNA world. *Chem. Biodiversity 4*, 633–655.

(5) Joyce, G. F. (2004) Directed evolution of nucleic acid enzymes. *Annu. Rev. Biochem. 73*, 791–836.

(6) Wilson, D. S., and Szostak, J. W. (1999) In vitro selection of functional nucleic acids. *Annu. Rev. Biochem. 68*, 611–647.

(7) Wecker, M., Smith, D., and Gold, L. (1996) In vitro selection of a novel catalytic RNA: Characterization of a sulfur alkylation reaction and interaction with a small peptide. *RNA 2*, 982–994.

(8) Wilson, C., and Szostak, J. W. (1995) In vitro evolution of a self-alkylating ribozyme. *Nature 374*, 777–782.

(9) Seelig, B., and Jaschke, A. (1999) A small catalytic RNA motif with Diels-Alderase activity. *Chem. Biol. 6*, 167–176.

(10) Sengle, G., Eisenfuhr, A., Arora, P. S., Nowick, J. S., and Famulok, M. (2001) Novel RNA catalysts for the Michael reaction. *Chem. Biol. 8*, 459–473.

(11) Fusz, S., Eisenfuhr, A., Srivatsan, S. G., Heckel, A., and Famulok, M. (2005) A ribozyme for the aldol reaction. *Chem. Biol. 12*, 941–950.

(12) Tsukiji, S., Pattnaik, S. B., and Suga, H. (2003) An alcohol dehydrogenase ribozyme. *Nat. Struct. Biol. 10*, 713–717.

(13) Tsukiji, S., Pattnaik, S. B., and Suga, H. (2004) Reduction of an aldehyde by a NADH/Zn^{2+}-dependent redox active ribozyme. *J. Am. Chem. Soc. 126*, 5044–5045.

(14) Cech, T. R. (2009) Crawling out of the RNA world. *Cell 136*, 599–602.

(15) Wilson, T. J., and Lilley, D. M. J. (2009) The evolution of ribozyme chemistry. *Science 323*, 1436–1438.

(16) Auld, D. S. (2001) Zinc coordination sphere in biochemical zinc sites. *BioMetals 14*, 271–313.

(17) Vallee, B. L., and Auld, D. S. (1990) Active-site zinc ligands and activated H_2O of zinc enzymes. *Proc. Natl. Acad. Sci. U.S.A. 87*, 220–224.

(18) Borda, E. J., Markley, J. C., and Sigurdsson, S. T. (2003) Zinc-dependent cleavage in the catalytic core of the hammerhead ribozyme: Evidence for a pH-dependent conformational change. *Nucleic Acids Res. 31*, 2595–2600.

(19) Markley, J. C., Godde, F., and Sigurdsson, S. T. (2001) Identification and Characterization of a Divalent Metal Ion-Dependent Cleavage Site in the Hammerhead Ribozyme. *Biochemistry 40*, 13849–13856.

(20) Cuzic, S., and Hartmann, R. K. (2005) Studies on *Escherichia coli* RNase P RNA with Zn^{2+} as the catalytic cofactor. *Nucleic Acids Res. 33*, 2464−2474.
(21) Brännvall, M., and Kirsebom, L. A. (2001) Metal ion cooperativity in ribozyme cleavage of RNA. *Proc. Natl. Acad. Sci. U.S.A. 98*, 12943−12947.
(22) Li, J., Zheng, W., Kwon, A. H., and Lu, Y. (2000) In vitro selection and characterization of a highly efficient Zn(II)-dependent RNA-cleaving deoxyribozyme. *Nucleic Acids Res. 28*, 481−488.
(23) Igloi, G. L. (1988) Interaction of tRNAs and of phosphorothioate-substituted nucleic acids with an organomercurial. Probing the chemical environment of thiolated residues by affinity electrophoresis. *Biochemistry 27*, 3842−3849.
(24) Putz, J., Wientges, J., Sissler, M., Giege, R., Florentz, C., and Schwienhorst, A. (1997) Rapid selection of aminoacyl-tRNAs based on biotinylation of α-NH_2 group of charged amino acids. *Nucleic Acids Res. 25*, 1862−1863.
(25) Wang, T.-P., Chiou, Y.-J., Chen, Y., Wang, E.-C., Hwang, L.-C., Chen, B.-H., Chen, Y.-H., and Ko, C.-H. (2010) Versatile Phosphoramidation Reactions for Nucleic Acid Conjugations with Peptides, Proteins, Chromophores, and Biotin Derivatives. *Bioconjugate Chem. 21*, 1642−1655.
(26) Unrau, P. J., and Bartel, D. P. (1998) RNA-catalysed nucleotide synthesis. *Nature 395*, 260−263.
(27) Mathews, D. H., Disney, M. D., Childs, J. L., Schroeder, S. J., Zuker, M., and Turner, D. H. (2004) Incorporating chemical modification constraints into a dynamic programming algorithm for prediction of RNA secondary structure. *Proc. Natl. Acad. Sci. U.S.A. 101*, 7287−7292.
(28) Rushizky, G. W., and Sober, H. A. (1963) Studies on the Specificity of Ribonuclease T2. *J. Biol. Chem. 238*, 371−376.
(29) Lee, N., and Suga, H. (2001) A minihelix-loop RNA acts as a trans-aminoacylation catalyst. *RNA 7*, 1043−1051.
(30) Ramaswamy, K., Wei, K., and Suga, H. (2002) Minihelix-loop RNAs: Minimal structures for aminoacylation catalysts. *Nucleic Acids Res. 30*, 2162−2171.
(31) Saito, H., Kourouklis, D., and Suga, H. (2001) An in vitro evolved precursor tRNA with aminoacylation activity. *EMBO J. 20*, 1797−1806.
(32) Kang, T. J., and Suga, H. (2007) In vitro selection of a 5′-purine nucleotide transferase ribozyme. *Nucleic Acids Res. 35*, 379−380.
(33) Daiyasu, H., Osaka, K., Ishino, Y., and Toh, H. (2001) Expansion of the zinc metallo-hydrolase family of the β-lactamase fold. *FEBS Lett. 503*, 1−6.
(34) Holland, D. R., Hausrath, A. C., Juers, D., and Matthews, B. W. (1995) Structural analysis of zinc substitutions in the active site of thermolysin. *Protein Sci. 4*, 1955−1965.
(35) Hernick, M., and Fierke, C. A. (2005) Zinc hydrolases: The mechanisms of zinc-dependent deacetylases. *Arch. Biochem. Biophys. 433*, 71−84.
(36) McCall, K. A., Huang, C., and Fierke, C. A. (2000) Function and mechanism of zinc metalloenzymes. *J. Nutr. 130*, 1437S−1446S.
(37) Nix, J., Sussman, D., and Wilson, C. (2000) The 1.3 Å crystal structure of a biotin-binding pseudoknot and the basis for RNA molecular recognition. *J. Mol. Biol. 296*, 1235−1244.
(38) Jaeger, L., Michel, F., and Westhof, E. (1994) Involvement of a GNRA tetraloop in long-range RNA tertiary interactions. *J. Mol. Biol. 236*, 1271−1276.